Front. Mech. Eng. 2023, 18(2): 19
https://doi.org/10.1007/s11465-022-0735-x

RESEARCH ARTICLE

Design and characteristic research of a novel electromechanical-hydraulic hybrid actuator with two transmission mechanisms

Shufei QIAO, Long QUAN (✉), Yunxiao HAO, Lei GE, Lianpeng XIA

Key Laboratory of Advanced Transducers and Intelligent Control System of Ministry of Education, Taiyuan University of Technology, Taiyuan 030024, China

✉ *Corresponding author. E-mail: quanlong@tyut.edu.cn (Long QUAN)*

ABSTRACT Servo-hydraulic actuators (SHAs) are widely used in mechanical equipment to drive heavy-duty mechanisms. However, their energy efficiency is low, and their motion characteristics are inevitably affected by uncertain nonlinearities. Electromechanical actuators (EMAs) possess superior energy efficiency and motion characteristics. However, they cannot easily drive heavy-duty mechanisms because of weak bearing capacity. This study proposes and designs a novel electromechanical-hydraulic hybrid actuator (EMHA) that integrates the advantages of EMA and SHA. EMHA mainly features two transmission mechanisms. The piston of the hydraulic transmission mechanism and the ball screw pair of the electromechanical transmission mechanism are mechanically fixed together through screw bolts, realizing the integration of two types of transmission mechanisms. The control scheme of the electromechanical transmission mechanism is used for motion control, and the hydraulic transmission mechanism is used for power assistance. Then, the mathematical model, structure, and parameter design of the new EMHA are studied. Finally, the EMHA prototype and test platform are manufactured. The test results prove that the EMHA has good working characteristics and high energy efficiency. Compared with the valve-controlled hydraulic cylinder system, EMHA exhibits a velocity tracking error and energy consumption reduced by 49.7% and 54%, respectively, under the same working conditions.

KEYWORDS electromechanical-hydraulic hybrid actuator (EMHA), integration, transmission mechanisms, power assistance, energy efficiency, working characteristics

1 Introduction

Linear actuators are important components of mechanical equipment. For example, driving aircraft undercarriage and flight control surfaces [1], angle adjustment of the rocket launch [2], and lifting manipulators configured on excavators [3], cranes [4], and wheel loaders [5] are inseparable from linear actuators.

The existing mechanical equipment is generally equipped with servo-hydraulic actuators (SHAs) because of their high power density and output force [6]. During operation, the control valve is used to control the velocity by distributing the pressure and flow of the hydraulic system into hydraulic cylinders, causing huge throttling loss and low energy efficiency [7]. Driven by the requirements of global low-carbon economies, many researchers improve energy efficiency by reducing throttling loss. For example, a load sensing system is adopted to balance the supply and demand flow by adjusting pump displacement according to the difference between the pump and load pressure, thereby reducing throttling loss [8,9]. Moreover, the independent metering system that decouples two chambers of the hydraulic cylinder is adopted to reduce throttling loss [10–12]. In one working cycle, the energy consumption of the excavator boom with the independent metering system can be reduced by 15% compared with that with the load sensing system [13]. The pump-controlled hydraulic cylinder technology is studied to eliminate throttling loss further; this technology cancels the control valve and uses a pump to control the hydraulic cylinder velocity directly [14]. The pump-controlled system is 50% more efficient

Received April 25, 2022; accepted August 22, 2022

than the independent metering system during the excavator boom extension process [15].

The development of mechatronics, integrated machinery, and power-by-wire technology has brought great interest to the electro-hydrostatic actuator (EHA) from some fields, such as aerospace, large commercial aircraft, and robotics [16,17]. EHA is an integrated modular actuator with high power density and energy efficiency because of the elimination of complicated pipelines and control valves with low energy efficiency [18]. EHA has been applied to drive ailerons and elevators of Airbus A380 and attack aircraft [19,20]. It has been also employed in wearable robots [21]. However, the single-rod hydraulic cylinder is favored for mechanical equipment because of its great output force. Thus, the pump-controlled system must be equipped with various hydraulic components to balance the asymmetric flow of the two chambers of the hydraulic cylinder [22]. In addition, the control characteristics of EHA are inevitably affected by nonlinear factors, such as pump response, oil compression, and leakage.

An electromechanical actuator (EMA), which transmits power through a rigid mechanical structure, can easily realize the accurate control of velocity, position, and force [23]. Compared with SHA, EMA eliminates throttling loss, and the electric energy is directly converted into mechanical energy. The energy conversion link is the least, and the energy efficiency is high [24]. EMAs are currently considered an alternative to conventional hydraulic cylinders in many industrial applications, including the aeronautic sector, because of their high efficiency and relatively simple commandability. EMA has been successfully adopted to drive the landing gear, brake, and spoiler of Boeing 787, the slat and horizontal stabilizer of Airbus A380 [25,26], and the legs of mobile robots [27]. The research of EMA mainly focuses on structural optimization and application. Caracciolo and Richiedei [28] proposed a model-based structural parameter design method of EMA, minimizing the installed power by matching the parameters of the motor and ball screw. Elduque et al. [29] reduced energy consumption by 15% by optimizing the process of the electric injection molding machine. However, the power density and bearing capacity of EMA are small. Thus, directly applying EMA in mechanical equipment to drive heavy-duty mechanisms is challenging. Therefore, Quan et al. [30,31] proposed an electrohydraulic hybrid drive system in which the EMA and hydraulic cylinders are arranged in parallel to drive the manipulator jointly. Compared with the traditional SHA system, the electrohydraulic hybrid drive system exhibits an energy consumption reduced by 51% and possesses excellent control characteristics.

The present study proposes and designs a novel electromechanical-hydraulic hybrid actuator (EMHA) to address the above challenges. The proposed EMHA has two power sources and transmission mechanisms. The electromechanical transmission mechanism is used for motion control, replacing the valve-controlled method with low energy efficiency. The hydraulic transmission mechanism is used for power assistance, thereby improving the bearing capacity of EMHA. The proposed EMHA has high energy efficiency and high output force at the same time.

This paper is organized as follows. First, the principle and control strategy of the proposed EMHA is analyzed in Section 2. In Section 3, the mathematical modeling and analysis of the proposed EMHA are carried out. In Section 4, the structure and parameters of EMHA are designed for prototype manufacturing. In Section 5, the test platform is constructed, and experiments are performed to prove the characteristics of EMHA. The conclusions are presented in Section 6.

2 Principle of EMHA

2.1 Distributed linear drive

Figure 1 shows the distributed electromechanical-hydraulic hybrid linear drive system. EMA, which has high energy efficiency and control performance, is used to control the load mechanism velocity. SHA, which has high power density and large output force, is used to overcome heavy load, assisting the motion drive of EMA. In the process of power assistance, SHA is used only for force compensation. It does not need to control the velocity and position through throttling.

As shown in Fig. 1, the distributed linear drive system adopts the form of a parallel arrangement of multiple actuators. In the double-actuator coupling drive mechanism shown in Fig. 1(a), the load mechanism is deformed because the load force F_{L} is not collinear with the output forces F_{E} and F_{H} of the two actuators. The load force transmitted to the driving rod through the load mechanism is not complete along the drive rod axis, and a certain angle θ exists. Therefore, the driving rods of EMA and SHA are subjected to radial forces $-F_{\mathrm{ER}}$ and $-F_{\mathrm{HR}}$, respectively, which can be written as Eq. (1).

$$\begin{cases} -F_{\mathrm{ER}} = -F_{\mathrm{E}} \tan\theta_{\mathrm{E}}, \\ -F_{\mathrm{HR}} = -F_{\mathrm{H}} \tan\theta_{\mathrm{H}}, \\ F_{\mathrm{E}} + F_{\mathrm{H}} = F_{\mathrm{L}}, \end{cases} \tag{1}$$

where F_{E} is the output force of EMA, F_{H} is the output force of SHA, θ_{E} is the angle between the load force of the EMA driving rod and the axis, and θ_{H} is the angle between the load force of the SHA driving rod and the axis.

Affected by radial forces, the driving rods of EMA and SHA are bent and deformed. Thus, the stuck phenomenon and the nonuniform wear of the sealing structure are aggravated. This phenomenon affects the service life and

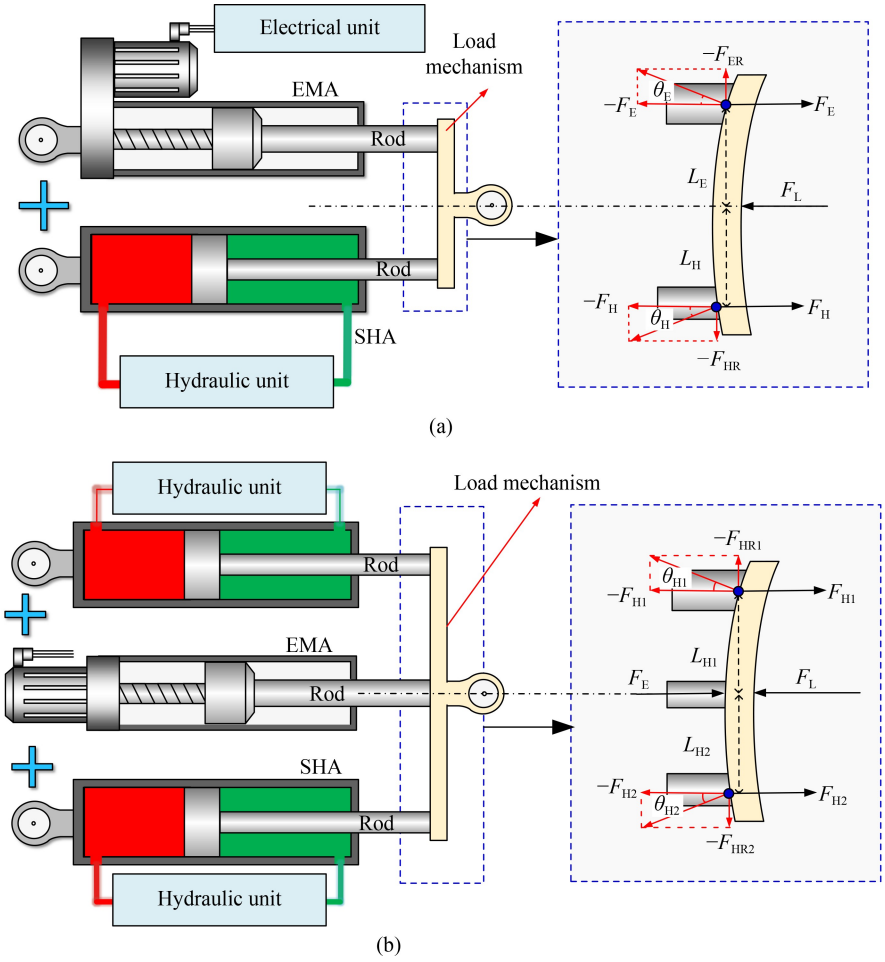

Fig. 1 Distributed electromechanical-hydraulic hybrid linear drive system: (a) double-actuator coupling drive mechanism and (b) symmetrical coupling drive mechanism with multiple actuators. EMA: electromechanical actuator, SHA: servo-hydraulic actuator.

reliability of actuators. In addition, this distributed linear drive mechanism has additional torque, written as Eq. (2). It also aggravates the nonuniform wear and motion jitter of the actuators. In the process of velocity change, the force of EMA suddenly increases or decreases because the inertial force of the manipulator is overcome by EMA. Thus, the adverse effect of radial force and additional torque is aggravated again.

$$T_{\text{add}} = F_{\text{E}}L_{\text{E}} - F_{\text{H}}L_{\text{H}}, \tag{2}$$

where T_{add} is the additional torque of the distributed linear drive system, L_{E} is the arm distance of the EMA output force, and L_{H} is the arm distance of the SHA output force.

For the symmetrical coupling drive mechanism with multiple actuators shown in Fig. 1(b), EMA is arranged in the middle, and the power-assisted actuators SHA are arranged symmetrically on both sides in parallel. The output force of EMA is collinear with the load force, avoiding the influence of radial force and unbalanced load torque. However, SHA is still affected by the unbalanced load torque and radial force.

In addition, the distributed linear drive mechanism has multiple actuators. Thus, a large space is required, and the mass of the system is increased.

2.2 Integrated linear drive

Based on the principle of distributed electromechanical-hydraulic hybrid linear drive system, this study integrates EMA and SHA through structural reorganization. Thus, a novel integrated EMHA is proposed, as shown in Fig. 2.

As shown in Fig. 2, the proposed EMHA has two power source units: electrical unit and hydraulic unit. It also has two transmission mechanisms: electromechanical transmission and hydraulic transmission. The electromechanical transmission mechanism is mainly composed of a servo motor, reducer, and screw transmission component, which includes a lead screw and nut. The hydraulic transmission mechanism mainly comprises a piston, piston rod, and sealing rings. The electrical unit and electromechanical transmission mechanism are used for velocity and position control. The hydraulic unit and hydraulic transmission mechanism output large force to assist motion control, thereby improving the bearing

capacity of EMHA. The hydraulic unit does not need to control the velocity and position through throttling. Thus, energy loss can be reduced.

Figure 3 shows the power flow diagram of EMHA.

First, the electrical unit energy $U{\cdot}I$ is converted into mechanical energy $n{\cdot}T$ of the motor. Then, torque T is amplified through the reducer, driving the lead screw to rotate. The rotary motion of the lead screw is further converted into the linear motion of the nut through the screw transmission pair. The nut rigidly transmits its motion power $v{\cdot}F_{\mathrm{e}}$ to the piston. Under the assistance of hydraulic unit energy $p{\cdot}q$, the piston power is increased to $v{\cdot}F_{\mathrm{sum}}$ to drive the load. Among them, U and I are the voltage and current of the electrical unit, respectively, n and T are the speed and torque of the motor, respectively, v is the velocity of EMHA, F_{e} is the electromechanical transmission mechanism force, p and q are the pressure and flow rates of the hydraulic unit, respectively, and F_{sum} is the total output force.

The working modes of EMHA are as follows:

(1) EMHA drives the load mechanism only under the action of the electrical unit and electromechanical transmission mechanism when the external load force is less than the bearing capacity threshold of the electromechanical transmission mechanism. The hydraulic unit does not assist it and only maintains the minimum power to compensate for the system flow.

(2) The pressure of the hydraulic unit increases continuously to assist the electromechanical transmission system when the external load force exceeds the bearing capacity threshold of the electromechanical transmission mechanism, thereby ensuring the bearing capacity of EMHA.

Given that EMHA has two independent power source units and two transmission mechanisms, EMHA has two safety redundancies. EMHA is degraded to EMA and continues to work under the electrical unit and electromechanical transmission mechanism for a period when the hydraulic system leaks and the high-pressure oil cannot be established, thereby ensuring the machine stops safely. When the power supply line of the electrical unit fails or the servo motor burns out, EMHA is degraded to a hydraulic cylinder actuator and continues to work under the hydraulic unit and hydraulic transmission mechanism.

The output forces of the electromechanical and hydraulic transmission mechanisms are coupled to the piston in the integrated linear drive mechanism, unlike the case in the distributed linear drive mechanism. Thus, EMHA is not affected by the additional torque and radial force if the piston axis line is collinear with the load force action line.

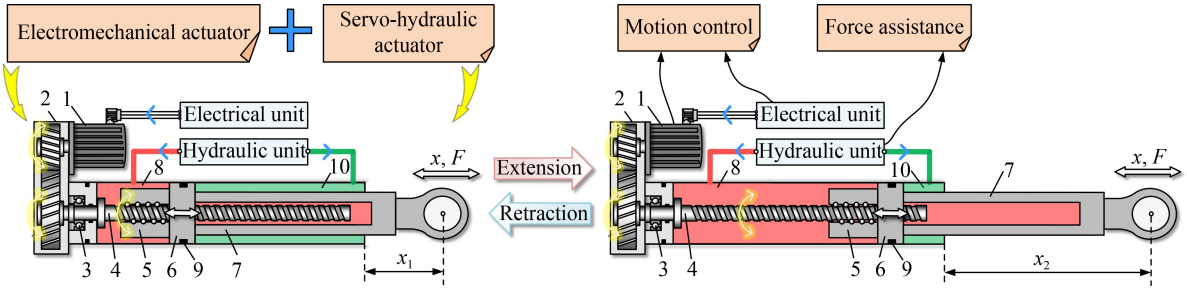

Fig. 2 Schematic diagram of electromechanical-hydraulic hybrid actuator. 1–servo motor, 2–reducer, 3–bearing, 4–lead screw, 5–nut, 6–piston, 7–piston rod, 8–rodless chamber, 9–sealing ring, 10–rod chamber.

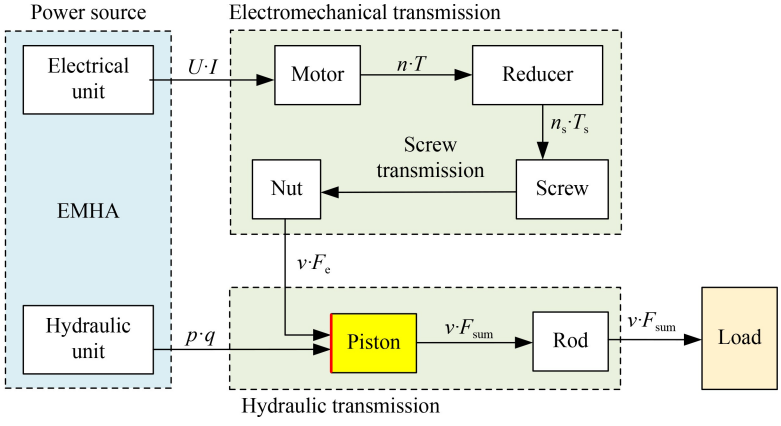

Fig. 3 Power flow diagram of electromechanical-hydraulic hybrid actuator (EMHA).

2.3 Control strategy

This study proposes a control scheme to ensure the dynamic coordination between the motor and the hydraulic unit and reduce the coupling effect between the electromechanical and hydraulic transmission systems. In this control scheme, the electromechanical transmission system is adopted for dynamic motion control. Moreover, the hydraulic transmission system is used for force control, thereby compensating for the force of the electromechanical transmission system. Thus, the decoupling of motion control and force control is realized. Figure 4 shows the overall control strategy between the two drive systems of EMHA.

As shown in Fig. 4, EMHA realizes the velocity and position control through the electromechanical transmission system. The servo motor of the electromechanical transmission system can realize the velocity closed-loop control of the actuator through the rotation speed feedback function of its encoder. The displacement closed-loop control of the actuator can be also realized through the external displacement sensor.

The hydraulic transmission system force controller outputs the target force control signal based on the torque threshold, the actual torque of the servo motor, and the pressure values of the hydraulic unit. The target pressure signal controls the pump pressure, actively adjusting the output force of the hydraulic transmission system. The output force of the hydraulic transmission system assists the electromechanical transmission system, thereby ensuring that the torque of the servo motor is less than the set torque threshold. The servo motor automatically compensates for the disturbance of the load force through the internal torque control loop when the pressure of the hydraulic unit changes. Thus, the load force balance is realized, and the coordination and stability of the system are ensured.

3 Mathematical modeling

Figure 5 is the simplified structure diagram of EMHA, which is beneficial to mathematical modeling and analysis.

The motion control equation of EMHA can be written as Eq. (3):

$$[x, v] = \frac{l}{k}\left[\frac{\alpha}{2\pi}, \frac{n}{60}\right], \tag{3}$$

where x is the displacement of EMHA, l is the lead of the screw transmission pair, k is the reduction ratio of the reducer, α is the rotation angle of the servo motor, and n is the rotation speed of the servo motor.

The reduction ratio k and lead l of EMHA are fixed values. Thus, the displacement x and velocity v of EMHA are proportional to the rotation angle α and rotation speed n of the servo motor. Therefore, realizing accurate motion control and automation through the servo drive technology of the servo motor is convenient.

The rotation angle of the servo motor is taken as the control variable. Thus, the electrical dynamic equation of the servo motor in d–q axes can be written as Eq. (4):

$$\begin{cases} J_e \dfrac{\mathrm{d}^2\alpha}{\mathrm{d}t^2} = N\psi i_q - B\dfrac{\mathrm{d}\alpha}{\mathrm{d}t} - T_L, \\ \dfrac{\mathrm{d}i_q}{\mathrm{d}t} = -\dfrac{Ri_q}{L_s} - Ni_d\dfrac{\mathrm{d}\alpha}{\mathrm{d}t} - \dfrac{N\psi}{L_s}\dfrac{\mathrm{d}\alpha}{\mathrm{d}t} + \dfrac{u_q}{L_s}, \\ \dfrac{\mathrm{d}i_d}{\mathrm{d}t} = -\dfrac{Ri_d}{L_s} + Ni_q\dfrac{\mathrm{d}\alpha}{\mathrm{d}t} + \dfrac{u_d}{L_s}, \end{cases} \tag{4}$$

where J_e is the moment of inertia driven by the electrical unit, t is time, N is the number of the pole pairs, ψ is the flux linkage amplitude of the rotor permanent magnet, i_q and i_d are the stator currents of the q axis and d axis, respectively, B is the rotational viscous friction coefficient, T_L is the equivalent load torque of the servo motor, R is the stator resistance, L_s is the equivalent inductance, and u_q and u_d are the stator voltages of the q axis and d axis.

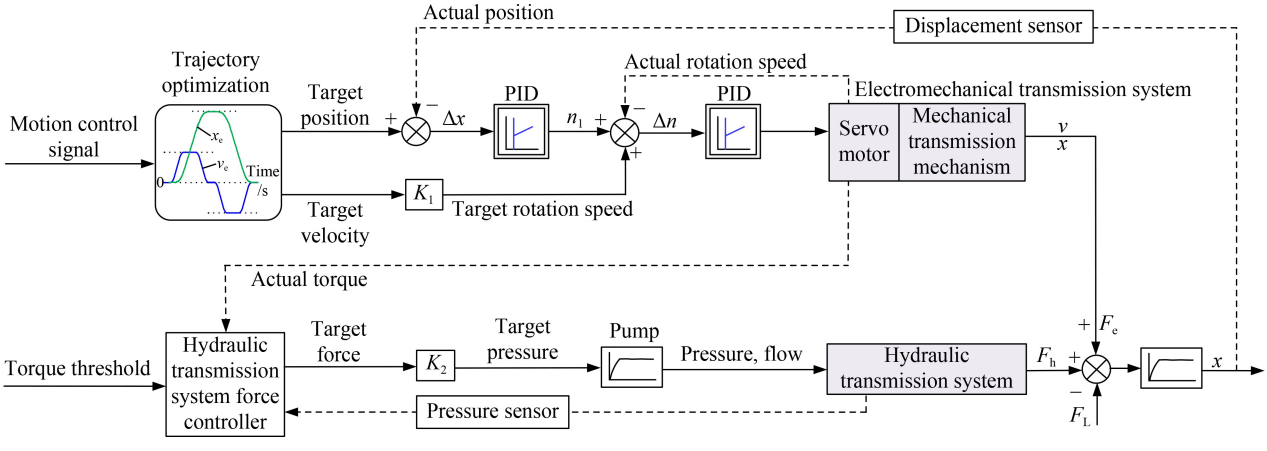

Fig. 4 Control strategy of electromechanical-hydraulic hybrid actuator.

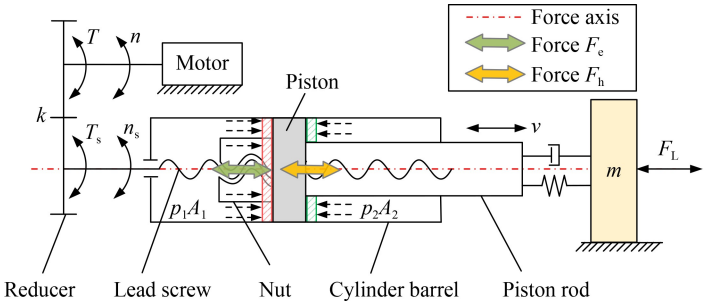

Fig. 5 Simplified structure diagram of electromechanical-hydraulic hybrid actuator.

In the process of motion control of the servo motor, particularly in the starting and braking stages, the system inertia influences the control characteristics of EMHA.

The equivalent moment of inertia J_L converted from the mass of load mechanism and hydraulic oil to lead screw can be written as Eq. (5):

$$J_L = \frac{(m_l + m_h) l^2}{4\pi^2}, \tag{5}$$

where m_l is the load mass, and m_h is the hydraulic oil mass.

The moment of inertia of the lead screw itself can be written as Eq. (6):

$$J_s = \frac{1}{8} m_s d_s^2 \times 10^{-6}, \tag{6}$$

where J_s is the moment of inertia of the lead screw, m_s is the lead screw mass, and d_s is the diameter of the lead screw.

Finally, the moment of inertia J_e driven by the electrical unit can be written as Eq. (7):

$$J_e = J_1 + J_2 + \frac{J_L + J_s}{k^2} = J_1 + J_2 + \frac{m_l + m_h}{4\pi^2}\left(\frac{l}{k}\right)^2 + \frac{J_s}{k^2}, \tag{7}$$

where J_1 and J_2 are the moments of inertia of the servo motor rotor and reducer, respectively.

According to Eq. (7), the larger the lead l of the screw transmission pair is, the greater the inertia overcome by the electrical unit is. The larger the reduction ratio k of the reducer is, the smaller the inertia overcome by the electrical unit is.

As shown in Fig. 5, the output force of the EMHA includes the electromechanical transmission mechanism force F_e and hydraulic transmission mechanism force F_h. The dynamic balance equation of the EMHA can be written as Eq. (8):

$$\begin{cases} F_e + F_h = m_l \dfrac{d^2x}{dt^2} + c\dfrac{dx}{dt} + F_L + F_f, \\ F_e = \dfrac{2\pi k T_L}{l}\eta_1, \\ F_h = (p_1A_1 - p_2A_2)\eta_2 \times 10^{-3}, \end{cases} \tag{8}$$

where c is the system viscous damping coefficient, F_f is the interference force including friction, η_1 and η_2 are the efficiencies of the mechanical and hydraulic transmission mechanism, respectively, p_1 and p_2 are the pressures of the EMHA rodless and rod chamber, respectively, and A_1 and A_2 are the effective action areas of the EMHA rodless and rod chamber pressure, respectively.

According to Eq. (8), part of the heavy load F_L can be overcome directly through the hydraulic transmission mechanism under the assistance of the hydraulic unit. The larger the pressure and the effective action area are, the more remarkable the hydraulic power assistance effect is, and the smaller the force of the electromechanical transmission mechanism outputs is. Thus, the force and dynamic torque of the electromechanical transmission mechanism can be considerably reduced because of the action of hydraulic power assistance.

4 Structure and parameter design

4.1 Structure design

The difficulties in the EMHA structure design include the integration of the hydraulic transmission mechanism and electromechanical transmission mechanism, building the high-pressure oil action chambers, and ensuring sealing performance of EMHA.

Figure 6 shows the three-dimensional structure diagram of the designed EMHA in this study.

4.1.1 Mechanical structure design

As shown in Fig. 6, the servo motor of the electromechanical transmission mechanism is arranged in parallel with the lead screw, and the power of the servo motor is transmitted to the lead screw through the gear reducer. The transition wheel is added to minimize the reducer size. In this way, the diameter and tooth width of the driving and the driven wheels can be reduced. The lead screw is divided into thread and nonthread parts. The thread part cooperates with the nut through the low-friction ball screw pair to convert the rotary motion into linear motion. The nonthread part includes the power input part and support part. The power input part is connected to the driven wheel through the flat key, and the support part is constrained by the thrust ball bearing.

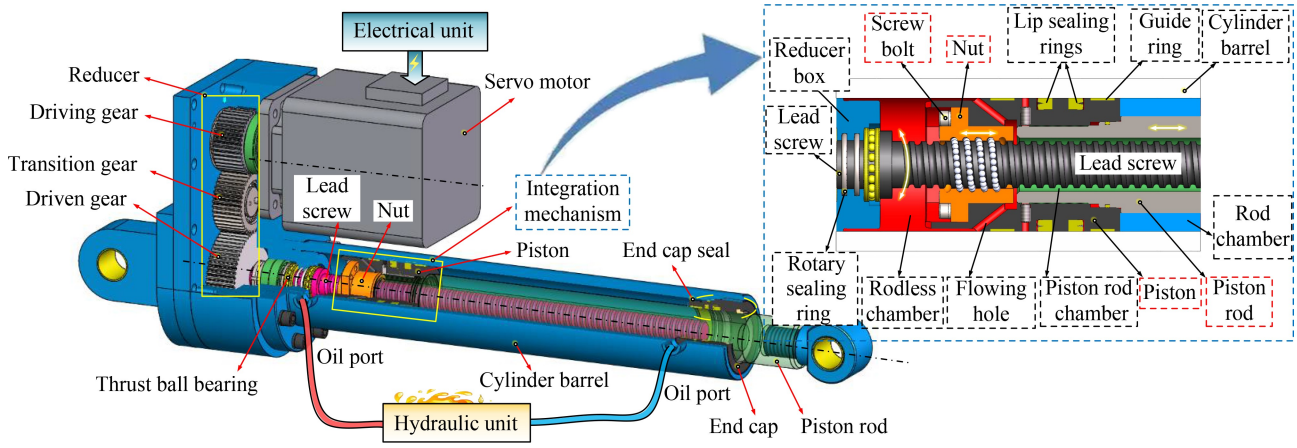

Fig. 6 Three-dimensional structure diagram of electromechanical-hydraulic hybrid actuator.

The force-amplifying component of the hydraulic transmission mechanism is the piston, and the linear output force component of the electromechanical transmission mechanism is the ball screw pair. Based on these characteristics, the piston component and the ball screw pair nut are mechanically fixed together through screw bolts, as shown in Fig. 6. Thus, the integration of the two transmission mechanisms is realized. Then, the piston and piston rod are assembled through the thread connection. Thus far, the nut of the electromechanical transmission mechanism is rigidly connected with the piston and piston rod of the hydraulic transmission mechanism, thereby forming the output mechanism of EMHA. Furthermore, the piston rod is designed as a hollow structure into which the lead screw is inserted to avoid installation interference between the lead screw and the piston rod. This cavity of the hollow piston rod is named the piston rod chamber.

4.1.2 Hydraulic oil chamber design

In this study, the hydraulic oil chambers are constructed on both sides of the piston. As shown in Fig. 6, two lip sealing rings with opposite lip directions are arranged between the piston and the cylinder barrel to seal the rodless chamber and rod chamber. The lip of the sealing ring is elastically deformed under the action of hydraulic oil to seal the gap between the piston and the cylinder barrel. The guide rings are used to prevent the piston from being scratched by supporting and guiding the linear motion of the piston. In addition, two rotary sealing rings are arranged at the place where the lead screw passes through the reducer box to prevent the pressure oil of the rodless chamber from leaking into the reducer.

The rodless chamber and piston rod chamber of EMHA are always in the state of oil connection because of the internal clearance of the ball screw pair. When EMHA moves rapidly, the hydraulic oil in the piston rod chamber and rodless chamber cannot flow rapidly because the internal clearance is small. In this scenario, cavitation or pressure holding problems occur easily. Thus, some holes for hydraulic oil flowing are designed on the piston, thereby ensuring that the hydraulic oil can flow rapidly. The hydraulic oil not only can realize the power assistance function but also can increase lubrication and reduce friction, thereby improving the transmission efficiency of EMHA.

4.2 Parameter matching

According to the previous research on the 6 t hydraulic excavator [30–32], the effective action areas of the rodless chamber and the rod chamber of the boom hydraulic cylinder actuator are 7850 and 4003 mm^2, respectively. The pressure of the rodless chamber and the rod chamber of the hydraulic cylinder is approximately 7 and 0.5 MPa, respectively, when the boom is lowered under no-load conditions. According to Eq. (8), the output force of the original hydraulic cylinder is approximately 53 kN. If the boom is lowered rapidly at the velocity of 150 mm/s, the driving power of the hydraulic cylinder is 8 kW, according to Eq. (9). If the boom is lifted under full load conditions, the pressure in the rodless chamber of the hydraulic cylinder is approximately 13 MPa. If the boom is lifted at the velocity of 150 mm/s, the driving power of the hydraulic cylinder is 15 kW.

$$P_{\mathrm{h}} = (p_1 A_1 - p_2 A_2)\, v, \tag{9}$$

where P_{h} is the driving power of the hydraulic cylinder.

According to the driving requirements of the excavator boom, this study carries out the parameter matching design of EMHA based on the following principle: The electromechanical transmission mechanism controls the movement of the boom under no-load conditions, and the hydraulic transmission mechanism assists the boom motion under full load conditions or excavation conditions. Given the principle of minimizing the installed power of the electromechanical transmission mechanism, the rated power of the servo motor is preliminarily

selected as 8 kW in this study to make the electromechanical transmission mechanism meet the requirements of boom driving. According to the actual stroke of the boom hydraulic cylinder of the 6 t excavator, the working stroke of the EMHA is selected as 600 mm.

According to the actual velocity of the excavator boom, the linear velocity of EMHA used to drive the excavator boom is taken as 150 mm/s, the ball screw pair lead l is taken as 10 mm/r, and the reducer reduction ratio k is taken as 1.5. According to Eq. (3), the servo motor rotation speed is 1350 r/min, and the lead screw rotation speed is 900 r/min. For rotary sealing rings, the allowable linear velocity under high-pressure conditions is generally 2000 mm/s. Thus, the diameter of the lead screw can be written as Eq. (10):

$$d_s = \frac{60v_s}{\pi n_s} \leqslant \frac{60\times 2000}{900\pi} = 42.44 \text{ mm}, \tag{10}$$

where v_s is the linear speed of the lead screw rotation, and n_s is the rotation speed of the lead screw.

According to the parameters of ball screw pair products and the specifications of rotary sealing rings, ball screw pair with a nominal diameter of 40 mm is adopted, as shown in Table 1.

Table 1 Parameters of the ball screw pair

Parameter	Value
Nominal diameter	40 mm
Nominal lead	10 mm
Diameter of ball	7.144 mm
Outer diameter of flange	93 mm
Rated static load	70.5 kN
Rated dynamic load	46.5 kN
Efficiency	92%

Table 1 shows that the rated dynamic load of the ball screw pair is 46.5 kN. According to Eq. (8), the torque of the servo motor should reach 49.34 N·m. According to the parameters of the servo motor products, the servo motor with a rated rotation speed of 1400 r/min and a rated torque of 55 N·m is selected. The parameters of the servo motor are shown in Table 2.

According to the design of the three-chamber hydraulic cylinder [32], the wall thickness of the hollow piston rod is preliminarily selected as 18 mm. The outer diameter d of the piston rod can be written as Eq. (11):

$$d > d_s + 18\times 2 = 40 + 18\times 2 = 76 \text{ mm}. \tag{11}$$

Given the specifications of sealing rings, the diameters of the piston rod, piston, and cylinder barrel are selected as 80, 110, and 140 mm, respectively. The hydraulic unit effective action areas of the rodless chamber and rod chamber are 9503 and 4476 mm^2, respectively, which are calculated by Eq. (12):

Table 2 Parameters of the servo motor

Parameter	Value
Rated torque	55 N·m
Rated rotation speed	1400 r/min
Rated power	8 kW
Rated current	16.6 A
Rated frequency	100 Hz
Torque constant	3.31 N·m/A
Rotor inertia	0.007 kg·m^2
Number of pole pairs	4
Resistance	0.97 Ω
Inductance	14.6 mH

$$[A_1, A_2] = \frac{\pi}{4}[d_1^2, d_1^2 - d_2^2], \tag{12}$$

where d_1 and d_2 are the diameters of the piston and piston rod, respectively.

Then, the wheelbase D_{z1} between the servo motor and the lead screw can be written as Eq. (13).

$$D_{z1} > \frac{D_e + d_c}{2} = \frac{225 + 140}{2} = 182.5 \text{ mm}, \tag{13}$$

where D_e is the servo motor width, and d_c is the outer diameter of the cylinder barrel.

The wheelbase D_{z2} between the driving gear and the driven gear can be calculated by Eq. (14) based on the 2.5 mm gear module m. The number of driving gear teeth and that of transition gear teeth are equal.

$$\begin{cases} D_{z2} = \dfrac{mz_1 + mz_3}{2} + mz_2 = \dfrac{3mz_1 + mz_3}{2}, \\ k = \dfrac{z_3}{z_1}, \end{cases} \tag{14}$$

where z_1 is the number of the driving teeth, z_2 is the number of the transition teeth, and z_3 is the number of the driven teeth.

Figure 6 shows that the wheelbase of the servo motor and the lead screw is equal to the wheelbase of the driving gear and the driven gear. Thus, simultaneous Eqs. (13) and (14) can obtain that the driving gear teeth $z_1 \geqslant 32.44$, which is finally selected as 40.

The parameters of the designed EMHA are shown in Fig. 7 and Table 3.

The power and bearing capacities of EMHA shown in Table 3 are taken as design objectives; thus, EMA needs to be equipped with a servo motor with a power of 42 kW. According to the existing products, the mass of the servo motor is more than 100 kg, and the mass of the whole EMA is approximately 280 kg, which is huge and costly.

4.3 Finite element simulation

Under the same external load condition, the finite element stress simulations of the ball screw component of the

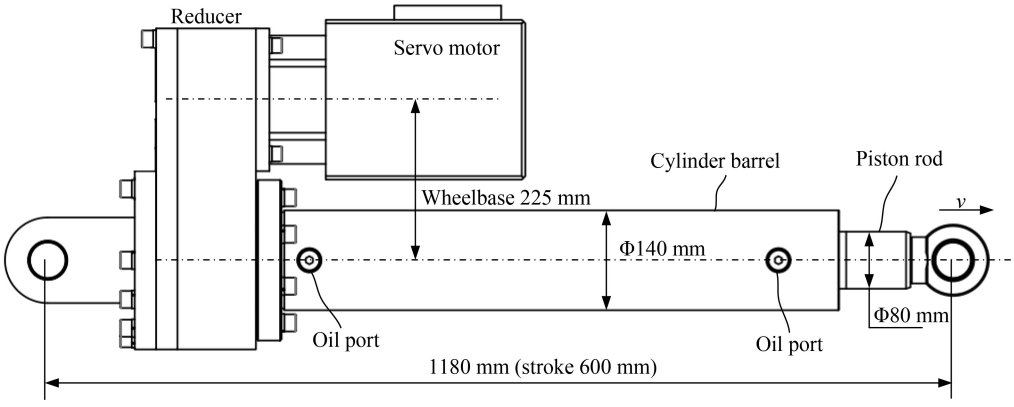

Fig. 7 Dimension diagram of electromechanical-hydraulic hybrid actuator.

Table 3 Parameters of EMHA

Parameter	Value
Velocity	150 mm/s
Maximum pressure	25 MPa
Maximum bearing capacity	280 kN
Power	42 kW
Mass	120 kg
Stroke	600 mm
Power density	0.35 kW/kg

nonhydraulic-assisted EMA and the hydraulic-assisted EMHA are performed through the software of ANSYS Workbench, shown in Fig. 8.

As shown in Fig. 8, the stress distribution of the ball screw component is mainly concentrated in the contact area between the ball and the spiral raceway. According to the stress isolines of EMHA, the maximum stress occurs at the contact point. It gradually decreases from the contact point to the surrounding. The maximum stress of the EMA lead screw is 824.87 MPa, and the maximum stress of the EMA ball is 670.09 MPa. Both exceed the allowable stress of the material and cannot drive a heavy load. Under the same heavy load, the maximum stress of the EMHA lead screw and ball is 217.95 and 179.32 MPa, respectively. These values are reduced by 73% and less than the allowable stress of the materials. Hydraulic

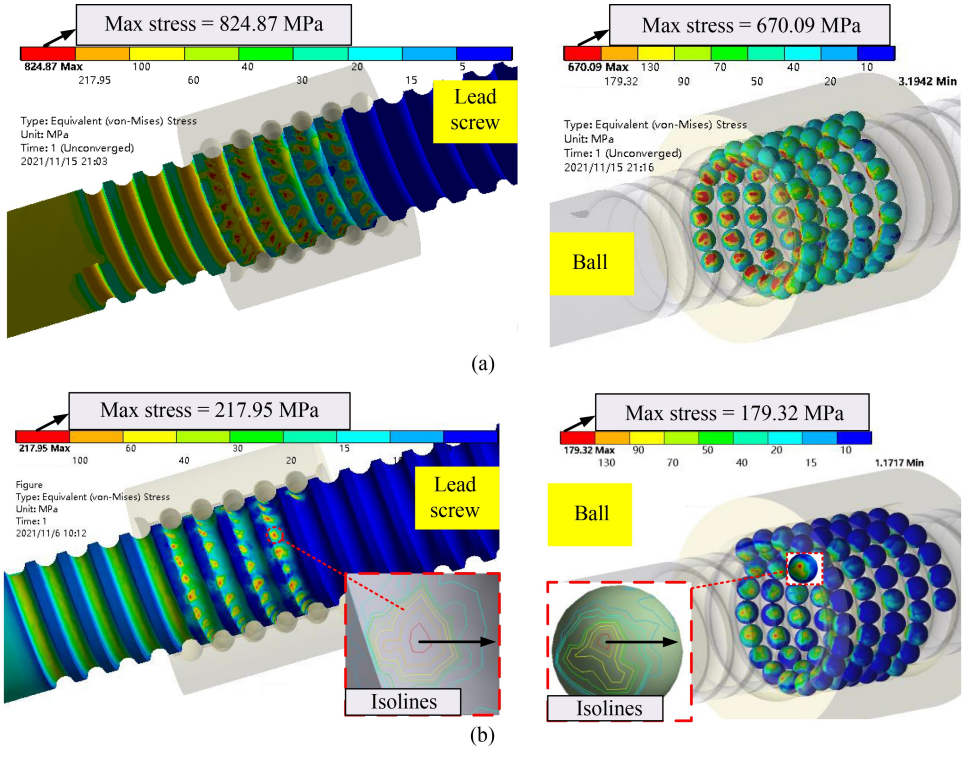

Fig. 8 Stress nephogram of the ball screw component: (a) electromechanical actuator with no hydraulic assistance and (b) electromechanical-hydraulic hybrid actuator with hydraulic assistance.

power assistance has a considerable effect on reducing the stress of the electromechanical transmission mechanism.

5 Experiment and result analysis

5.1 Test system

An actuator prototype was manufactured to study the actual characteristics of the proposed EMHA. The characteristics and energy efficiency of EMHA were tested using the test system shown in Fig. 9.

As shown in Fig. 9, the test system includes the EMHA driving system, loading system, signal acquisition system, and control system. The details of this test system are as follows:

(1) The electrical unit of EMHA adopts the Kollmorgen AKD series driver to control the servo motor. The hydraulic unit adopts a valve-controlled system comprising an oil tank, motor, variable pump, and proportional valve.

(2) The pressure of the loading cylinder is changed by adjusting the proportional reduction valve to realize the regulation of the load force. The loading cylinder is connected with EMHA through the car to realize loading.

(3) The signal acquisition system includes a pull wire displacement sensor for actuator displacement measurement, HYDAC pressure sensors for detecting the pressure of the two chambers of the actuator and the variable pump, and a WT3000 power meter for motor power detection.

(4) The control system adopts MicroLabBox 1202 hardware in the loop control system of dSPACE company in Germany to control the whole test system and collect real-time signals.

(5) During the test, the electromechanical-hydraulic hybrid linear drive mode is EMHA's working mode; that is, the electromechanical transmission mechanism is used for motion control, and the hydraulic transmission system is used for power assistance.

Based on the principle of the test system, the test platform is constructed as shown in Fig. 10.

5.2 Test results

First, the motion control characteristics of the traditional EMA and the new EMHA prototype are tested. Figure 11 shows the test result curves.

Given that the rotation speed step signals to the servo motor are 400 and 800 r/min, the corresponding linear target velocity of the actuator is 44.4 and 88.9 mm/s, according to Eq. (3). As shown in Fig. 11(a), the dynamic response time of EMA and EMHA from static to target velocity of 44.4 mm/s is approximately 50 and 47 ms respectively. The dynamic response time of EMA and EMHA from static to target velocity of 88.9 mm/s is approximately 89 and 87 ms, respectively. The dynamic response of EMHA is slightly faster than that of the traditional EMA because, under the same load conditions, the load inertia driven by the electromechanical transmission system of EMHA is reduced with the assistance of the hydraulic transmission system. During the movement, both actuators have no obvious velocity overshoot and fluctuation. The final velocity error of EMA and EMHA are 0.3 and 0.33 mm/s.

Given the position step signals 150 and 200 mm to EMA and EMHA, both actuators can run smoothly to the

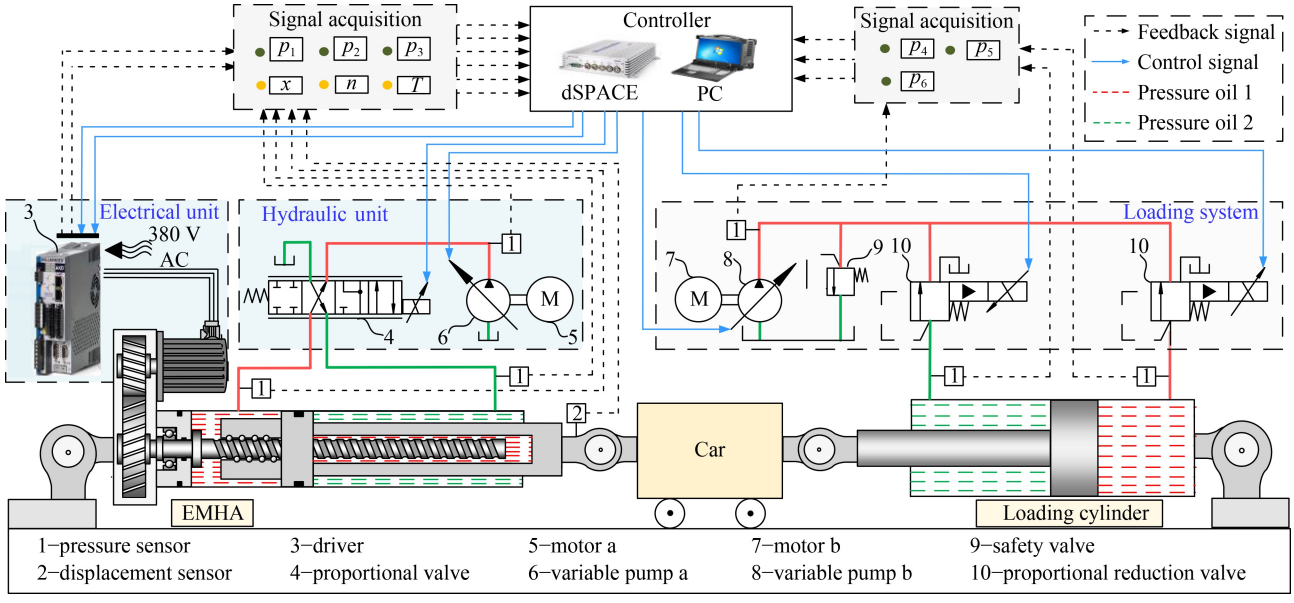

Fig. 9 Schematic diagram of the test system.

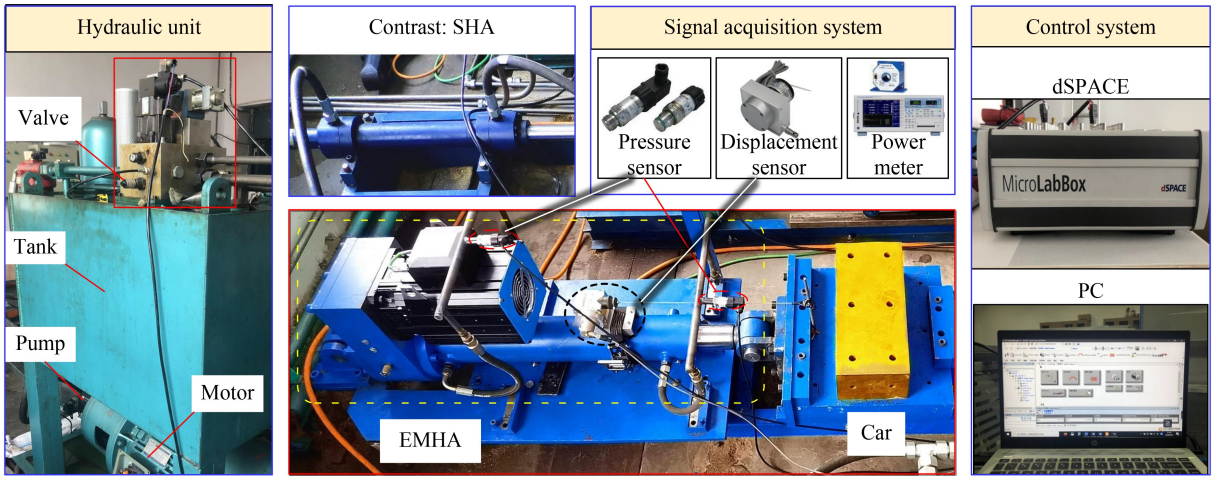

Fig. 10 Photograph of the test platform for linear actuator. EMHA: electromechanical-hydraulic hybrid actuator, SHA: servo-hydraulic actuator.

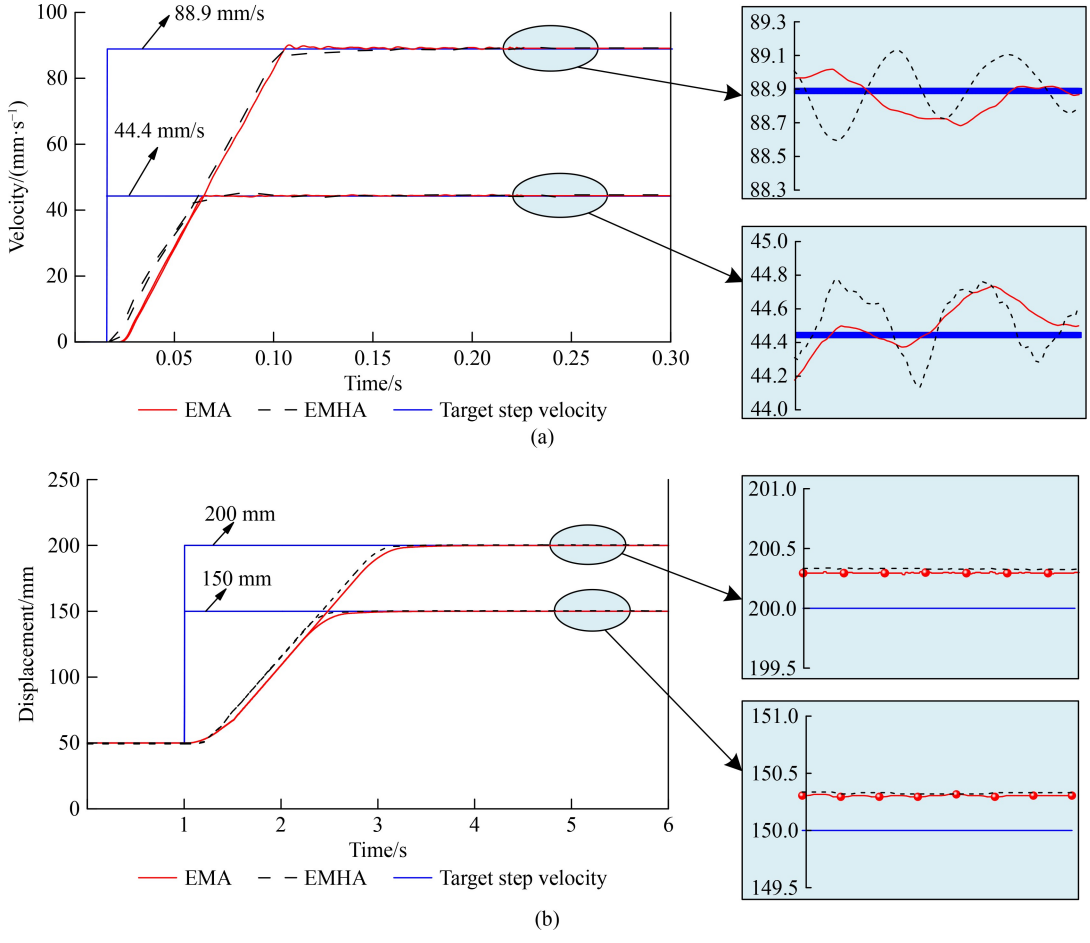

Fig. 11 Motion control characteristic curves: (a) velocity step characteristic and (b) position step characteristic. EMA: electromechanical actuator, EMHA: electromechanical-hydraulic hybrid actuator.

target position without any overshoot and fluctuation, as shown in Fig. 11(b). The final position error of EMA and EMHA are 0.32 and 0.37 mm.

According to the above test results, the motion control characteristics of EMHA are the same as those of EMA. Thus, the advantages of good control characteristics of EMA are retained. The reason is that the motion control of EMHA is also realized through the servo motor and the mechanical transmission mechanism.

Then, the working characteristics and energy efficiency

of the traditional SHA and the proposed EMHA prototype are tested separately under the same four-quadrant working conditions of resistive extension, exceeding retraction, exceeding extension, and resistive retraction. As shown in Figs. 9 and 10, the hydraulic circuit adopted by SHA in the test is the same as that of EMHA. Both are valve-controlled systems. The motor drives the variable pump to output high-pressure oil, which is input to the hydraulic cylinder through the proportional valve and drives the hydraulic cylinder working. Figure 12 shows the tracking characteristic curves of SHA and EMHA along the expected velocity and displacement trajectory signals.

As shown in Fig. 12, the actual displacements of SHA and EMHA are coincident with the expected displacement trajectories. However, the velocity gain of the SHA bidirectional motion is different because of the different action areas of the two chambers of the single-rod hydraulic cylinder, which is widely used in construction machinery. Thus, the velocity and position control characteristics of SHA are not symmetrical during the extension and retraction. As shown in Figs. 12(a) and 12(c), the difference between the actual velocity and the expected velocity is large during the retraction of SHA, and the maximum value is 14.7 mm/s. In addition, velocity fluctuations exist during the exceeding extension of SHA. The reason is that the motion control characteristics of SHA are affected by nonlinear factors, such as oil compression, oil leakage, pump response, and valve response.

The motion control of EMHA is realized by a mature servo motor drive technology and a rigid mechanical transmission mechanism. The bidirectional velocity gain of the servo motor is the same, and no factors, such as oil compression and leakage, exist. As shown in Figs. 12(b) and 12(c), the difference between the actual velocity and the expected velocity of EMHA is small, and the maximum value is 7.4 mm/s. The maximum velocity value of EMHA is 49.7% less than that of SHA. The working characteristics are remarkably improved.

Figure 13 shows the hydraulic system pressure characteristic curves of SHA and EMHA during the operation.

As shown in Fig. 13(a), the pressure difference between the pump and the rodless chamber of SHA during the working condition of resistive extension is 6.8 MPa. In particular, the pressure loss caused by the proportional valve is 6.8 MPa. Thus, the control characteristics of SHA shown in Fig. 12 are realized at the cost of energy loss. During the working condition of resistive extension, the pressure difference between the pump and the rodless

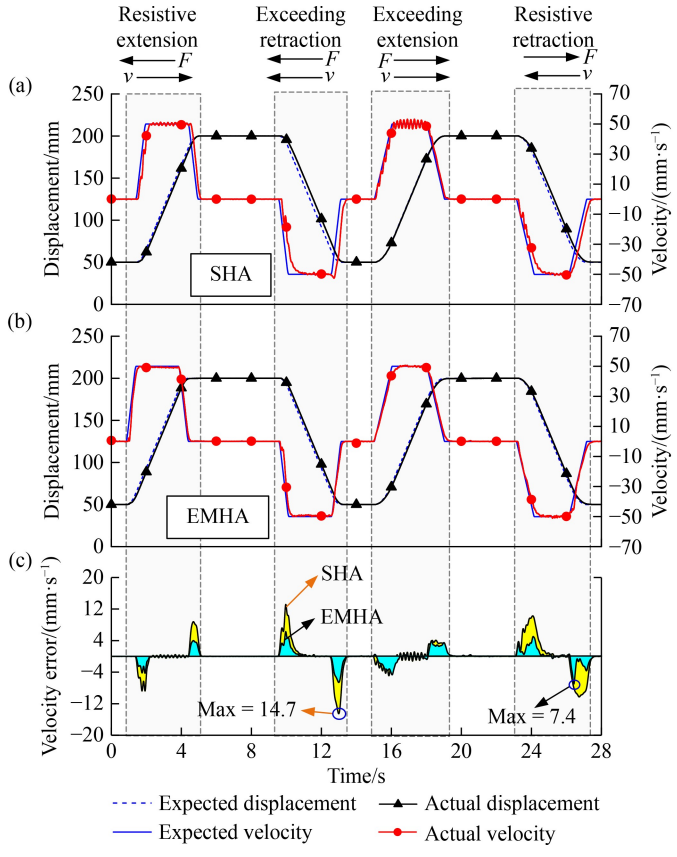

Fig. 12 Velocity and displacement tracking characteristic curves of actuators: (a) velocity and displacement tracking characteristic curves of servo-hydraulic actuator (SHA), (b) velocity and displacement tracking characteristic curves of electromechanical-hydraulic hybrid actuator (EMHA), and (c) velocity error characteristic curves.

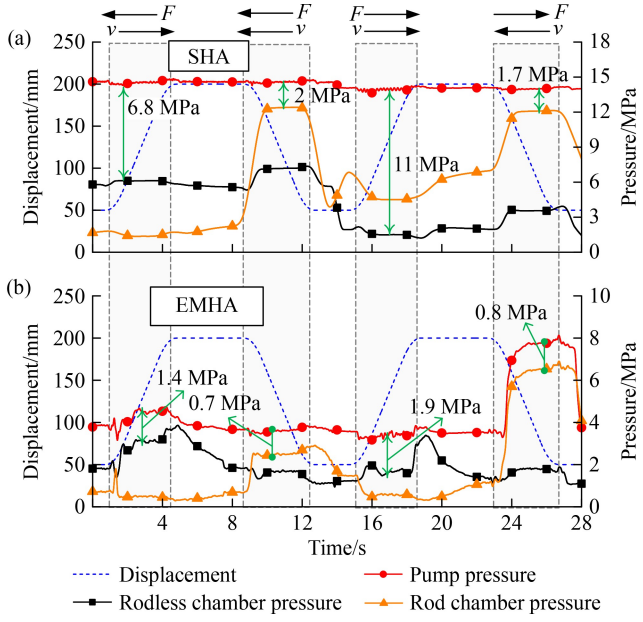

Fig. 13 Pressure characteristic curves of actuators: (a) pressure characteristic curves of servo-hydraulic actuator (SHA) and (b) pressure characteristic curves of electromechanical-hydraulic hybrid actuator (EMHA).

chamber of EMHA is less than 1.4 MPa, as shown in Fig. 13(b). This finding indicates that compared with SHA, EMHA exhibits pressure loss of the proportional valve that is reduced by 79%. Similarly, the pressure loss of EMHA under the working conditions of exceeding retraction, exceeding extension, and resistive retraction is smaller than that of SHA by 65%, 82%, and 53%, respectively. The energy throttling loss of EMHA is remarkably lower than that of the traditional SHA. The reason is that the velocity of EMHA is controlled by the electromechanical transmission mechanism. The proportional valve of the hydraulic unit mainly controls the flow direction of oil. It does not need to control the velocity and displacement of the EMHA through the opening size. Thus, the valve opening is large, and the throttling loss is small.

Then, the energy consumption characteristics of SHA and EMHA are shown in Fig. 14.

Under the four-quadrant working conditions, the peak power of the valve-controlled SHA system is 7.9 kW, the peak power of the EMHA servo motor is 1.2 kW, and the peak power of the EMHA hydraulic unit is 2.7 kW, as shown in Fig. 14. According to the test data, the total peak power of the EMHA system is 3.5 kW, which is less than that of the valve-controlled SHA system by 55.7%. In addition, during the whole working process, the energy consumption of the valve-controlled SHA system is 83.2 kJ, the energy consumption of the EMHA hydraulic unit is 26.8 kJ, and the energy consumption of the electrical unit is 11.5 kJ. Thus, the total energy consumption of the EMHA system is 38.3 kJ, which is less than that of the valve-controlled SHA system by 54%. The energy efficiency of EMHA is obviously improved.

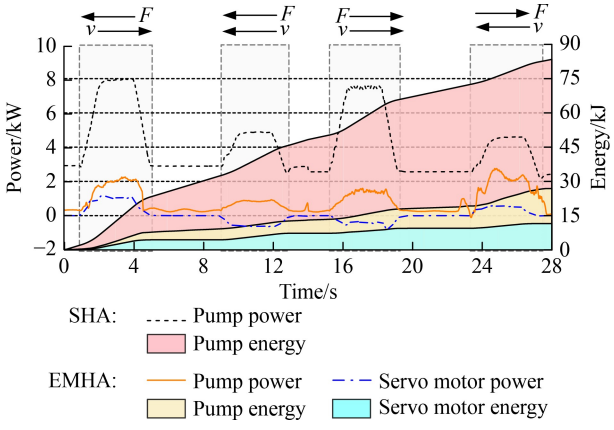

Fig. 14 Energy consumption characteristic curves. SHA: servo-hydraulic actuator, EMHA: electromechanical-hydraulic hybrid actuator.

According to Eq. (8), the electromechanical transmission mechanism output force is calculated based on the torque feedback of the servo motor, and the hydraulic transmission mechanism output force is calculated based on the pressure of the two chambers. The force distribution curves of each transmission mechanism of EMHA in the static state are shown in Fig. 15.

As shown in Fig. 15, the external load force increases from 0.4 s and stabilizes at 80 kN in 1.3 s. During the increase in the load force, the output force of the EMHA hydraulic transmission mechanism gradually increases to 72 kN, overcoming the external load. The average output force of the electromechanical transmission mechanism is only approximately 12 kN, which is only used to compensate for the output force of the hydraulic

transmission mechanism and overcome the interference force, such as system friction. The force of the hydraulic transmission mechanism is six times that of the electromechanical transmission mechanism. The assistance effect is remarkable.

Figure 16 shows the dynamic test characteristic curves of EMHA.

During the dynamic acceleration of the EMHA prototype, the external load force is adjusted from 28 to 52 kN through the loading system, as shown in Fig. 16. The increased load force is mainly overcome by the electromechanical transmission mechanism at the initial time because of the hysteresis of the hydraulic unit assistance. Moreover, the peak force of the electromechanical transmission mechanism is 41.5 kN. The rapid improvement of the hydraulic power assistance increases the output force of the hydraulic transmission mechanism to 45 kN and decreases the output force of the electromechanical transmission mechanism to 9.6 kN. The proportion of hydraulic power assistance is 82.4%. In the stage of uniform motion, the output force of each transmission mechanism is stable and has no vibration. After the EMHA stops moving, the test curve of the load disturbance stage in Fig. 16 shows that when the external load force has a large dynamic disturbance, the output force of the electromechanical transmission mechanism can quickly adapt to the load force changes because of the excellent torque compensation performance of the servo motor, thereby keeping load balance and system stability. Thus, good load disturbance coordination performance is acquired.

According to the test results, the performance values of EMHA are shown in Table 4.

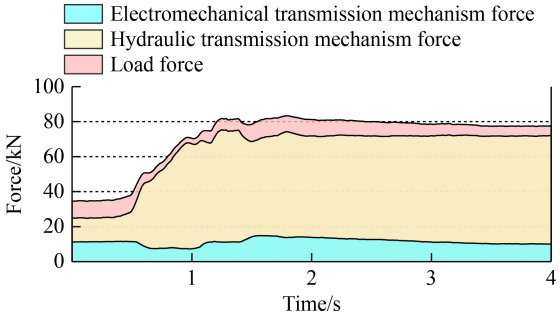

Fig. 15 Force curves of the electromechanical-hydraulic hybrid actuator transmission mechanisms.

6 Conclusions

(1) This study proposed, designed, and researched a novel EMHA to solve the problems of the existing linear drive system. This EMHA has two power sources and two transmission mechanisms. The electromechanical transmission mechanism with high energy efficiency is used to control velocity and displacement. The hydraulic transmission mechanism with high power density is used for power assistance, thereby improving the driving force of EMHA. In hydraulic assistance, the hydraulic unit does not need to control the velocity and position through throttling. Thus, energy loss is reduced.

(2) The test results show that the motion control characteristics of EMHA are the same as those of EMA.

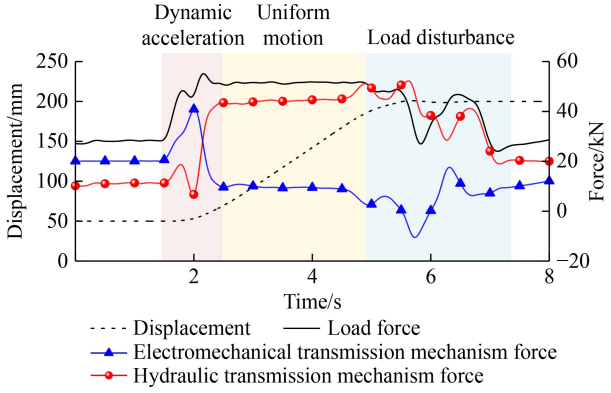

Fig. 16 Dynamic test characteristic curves of electromechanical-hydraulic hybrid actuator.

Table 4 Performance values of EMHA

Parameter	Value	Remark column
Dynamic response time	47 ms	Velocity step of 44.4 mm/s
Dynamic response time	87 ms	Velocity step of 88.9 mm/s
Velocity error	7.4 mm/s	Acceleration and deceleration phase
Velocity error	0.33 mm/s	Uniform motion stage
Positioning error	0.37 mm	–
Peak power of servo motor	1.2 kW	Four-quadrant working conditions
Peak power of hydraulic system	2.7 kW	Four-quadrant working conditions
Total energy consumption	38.3 kJ	Four-quadrant working conditions
Energy conservation	54%	Compared with the valve-controlled hydraulic cylinder system
Hydraulic power ratio	> 80%	Movement stage

Thus, the good control characteristics of EMA are retained. The actual displacement is coincident with the expected displacement trajectory. Compared with the traditional valve-controlled hydraulic cylinder system, EMHA exhibits a velocity tracking error reduced by 49.7%, peak power reduced by 55.7%, energy consumption reduced by 54%, and remarkably improved energy efficiency.

(3) The proposed EMHA integrates the advantages of SHA and EMA, and can achieve high energy efficiency and high power density driving. Thus, theoretical support for designing and manufacturing new linear actuators is provided.

Future work will focus on optimizing the structure, parameter, and coupling control strategy of EMHA.

Nomenclature

Abbreviations

EHA	Electro-hydrostatic actuator
EMA	Electromechanical actuator
EMHA	Electromechanical-hydraulic hybrid actuator
SHA	Servo-hydraulic actuator

Variables

A_1, A_2	Effective action areas of the EMHA rodless and rod chamber pressure, respectively
B	Rotational viscous friction coefficient
c	System viscous damping coefficient
d	Outer diameter of the piston rod
d_c	Outer diameter of the cylinder barrel
d_s	Diameter of the lead screw
d_1, d_2	Diameters of the piston and piston rod, respectively
D_e	Servo motor width
D_{z1}	Wheelbase between the servo motor and the lead screw
D_{z2}	Wheelbase between the driving gear and the driven gear
F_e	Electromechanical transmission mechanism force
F_E	Output force of EMA
F_{ER}	Radial force of the driving rod of EMA
F_f	Interference force including friction
F_h	Hydraulic transmission mechanism force
F_H	Output force of SHA
F_{HR}	Radial force of the driving rod of SHA
F_L	Load force
F_{sum}	Total output force
i_d	Stator current of the d axis
i_q	Stator current of the q axis
I	Current of the electrical unit
J_1, J_2	Moments of inertia of the servo motor rotor and reducer, respectively
J_e	Moment of inertia driven by the electrical unit
J_L	Equivalent moment of inertia of the load
J_s	Moment of inertia of the lead screw
k	Reducer reduction ratio
l	Lead of the screw transmission pair
L_E	Arm distance of the EMA output force
L_H	Arm distance of the SHA output force
L_s	Equivalent inductance
m	Gear module
m_h	Hydraulic oil mass
m_l	Load mass
m_s	Lead screw mass
n	Rotation speed of the servo motor
n_s	Rotation speed of the lead screw
N	Number of the pole pairs
p_1, p_2	Pressures of the EMHA rodless and rod chamber, respectively
P_h	Driving power of the hydraulic cylinder
R	Stator resistance
T	Torque amplified through the reducer
T_{add}	Additional torque of the distributed linear drive system
T_L	Equivalent load torque of the servo motor
u_d	Stator voltage of the d axis
u_q	Stator voltage of the q axis
U	Voltage of electrical unit
v	Velocity of EMHA
v_s	Linear speed of the lead screw rotation
x	Displacement of EMHA
z_1, z_2, z_3	Numbers of the driving teeth, transition teeth, and driven teeth, respectively
α	Rotation angle of the servo motor
ψ	Flux linkage amplitude of the rotor permanent magnet
η_1, η_2	Efficiency of the mechanical and hydraulic transmission mechanism, respectively
θ	A certain angle
θ_E	Angle between the load force of the EMA driving rod and axis
θ_H	Angle between the load force of the SHA driving rod and axis

Acknowledgements This work was supported by the National Natural Science Foundation of China (Grant Nos. 51875385 and 51805349).

References

1. Wang Y, Guo S R, Dong H K. Modeling and control of a novel electro-hydrostatic actuator with adaptive pump displacement.

Chinese Journal of Aeronautics, 2020, 33(1): 365–371
2. Li B, Rui X T, Tian W, Cui G Y. Neural-network-predictor-based control for an uncertain multiple launch rocket system with actuator delay. Mechanical Systems and Signal Processing, 2020, 141: 106489
3. Xu B, Cheng M. Motion control of multi-actuator hydraulic systems for mobile machineries: recent advancements and future trends. Frontiers of Mechanical Engineering, 2018, 13(2): 151–166
4. Jensen K J, Ebbesen M K, Hansen M R. Anti-swing control of a hydraulic loader crane with a hanging load. Mechatronics, 2021, 77: 102599
5. Wang X Y, Yang J, Quan L, Zhang X G, Wang J. A novel high-efficiency wheel loader power steering system with fault-tolerant capability. IEEE Transactions on Vehicular Technology, 2018, 67(10): 9273–9283
6. Cibicik A, Pedersen E, Egeland O. Dynamics of luffing motion of a flexible knuckle boom crane actuated by hydraulic cylinders. Mechanism and Machine Theory, 2020, 143: 103616
7. Yao J Y. Model-based nonlinear control of hydraulic servo systems: challenges, developments and perspectives. Frontiers of Mechanical Engineering, 2018, 13(2): 179–210
8. Cheng M, Zhang J H, Xu B, Ding R Q. An electrohydraulic load sensing system based on flow/pressure switched control for mobile machinery. ISA Transactions, 2020, 96: 367–375
9. Bertolin M, Vacca A. An energy efficient power-split hybrid transmission system to drive hydraulic implements in construction machines. Journal of Dynamic Systems, Measurement, and Control, 2021, 143(10): 101005
10. Lyu L T, Chen Z, Yao B. Energy saving motion control of independent metering valves and pump combined hydraulic system. IEEE/ASME Transactions on Mechatronics, 2019, 24(5): 1909–1920
11. Ding R Q, Xu B, Zhang J H, Cheng M. Bumpless mode switch of independent metering fluid power system for mobile machinery. Automation in Construction, 2016, 68: 52–64
12. Zhong Q, Bao H M, Li Y B, Hong H C, Zhang B, Yang H Y. Investigation into the independent metering control performance of a twin spools valve with switching technology-controlled pilot stage. Chinese Journal of Mechanical Engineering, 2021, 34(1): 91
13. Dong Z X, Huang W N, Ge L, Quan L, Huang J H, Yang J. Research on the performance of hydraulic excavator with pump and valve combined separate meter in and meter out circuits. Journal of Mechanical Engineering, 2016, 52(12): 173–180
14. Fassbender D, Zakharov V, Minav T. Utilization of electric prime movers in hydraulic heavy-duty-mobile-machine implement systems. Automation in Construction, 2021, 132: 103964
15. Ge L, Quan L, Li Y W, Zhang X G, Yang J. A novel hydraulic excavator boom driving system with high efficiency and potential energy regeneration capability. Energy Conversion and Management, 2018, 166: 308–317
16. Fu J, Mare J C, Yu L M, Fu Y L. Multi-level virtual prototyping of electromechanical actuation system for more electric aircraft. Chinese Journal of Aeronautics, 2018, 31(5): 892–913
17. Henderson J P, Plummer A, Johnston N. An electro-hydrostatic actuator for hybrid active-passive vibration isolation. International Journal of Hydromechatronics, 2018, 1(1): 47–71
18. Cai Y, Ren G, Song J C, Sepehri N. High precision position control of electro-hydrostatic actuators in the presence of parametric uncertainties and uncertain nonlinearities. Mechatronics, 2020, 68: 102363
19. Lee W, Li S L, Han D, Sarlioglu B, Minav T A, Pietola M. A review of integrated motor drive and wide-bandgap power electronics for high-performance electro-hydrostatic actuators. IEEE Transactions on Transportation Electrification, 2018, 4(3): 684–693
20. Shang Y X, Li X B, Qian H, Wu S, Pan Q X, Huang L G, Jiao Z X. A novel electro hydrostatic actuator system with energy recovery module for more electric aircraft. IEEE Transactions on Industrial Electronics, 2020, 67(4): 2991–2999
21. Staman K, Veale A J, van der Kooij H. The PREHydrA: a passive return, high force density, electro-hydrostatic actuator concept for wearable robotics. IEEE Robotics and Automation Letters, 2018, 3(4): 3569–3574
22. Ren G, Costa G K, Sepehri N. Position control of an electro-hydrostatic asymmetric actuator operating in all quadrants. Mechatronics, 2020, 67: 102344
23. Shin H, Paul S, Jang D, Chang J, Yun Y, Kim Y. Practical consideration and testing of superior high force electromechanical actuator for electrically driven lathe. Mechatronics, 2021, 79: 102664
24. Mesalhy O, Elsayed M L, Corona J J, Kwarteng A A, Kizito J P, Leland Q H, Chow L C. Study of a high-reliability dual-fan system for cooling aerospace electromechanical actuators. Thermal Science and Engineering Progress, 2020, 18: 100540
25. Qiao G, Liu G, Shi Z H, Wang Y W, Ma S J, Lim T C. A review of electromechanical actuators for more/all electric aircraft systems. Proceedings of the Institution of Mechanical Engineers, Part C: Journal of Mechanical Engineering Science, 2018, 232(22): 4128–4151
26. Zhang Y J, Liu L S, Peng Y, Liu D T. An electro-mechanical actuator motor voltage estimation method with a feature-aided Kalman filter. Sensors, 2018, 18(12): 4190
27. Liu J M, Tian Y, Gao F. A novel six-legged walking machine tool for *in-situ* operations. Frontiers of Mechanical Engineering, 2020, 15(3): 351–364
28. Caracciolo R, Richiedei D. Optimal design of ball-screw driven servomechanisms through an integrated mechatronic approach. Mechatronics, 2014, 24(7): 819–832
29. Elduque A, Elduque D, Javierre C, Fernández Á, Santolaria J. Environmental impact analysis of the injection molding process: analysis of the processing of high-density polyethylene parts. Journal of Cleaner Production, 2015, 108: 80–89
30. Hao Y, Xia L, Ge L, Wang X, Quan L. Position control performance of hydraulic electric hybrid linear drive system. Transactions of the Chinese Society for Agricultural Machinery, 2020, 51(3): 379–385 (in Chinese)
31. Li Z P, Wang C W, Quan L, Hao Y X, Ge L, Xia L P. Study on energy efficiency characteristics of the heavy-duty manipulator driven by electro-hydraulic hybrid active-passive system. Automation in Construction, 2021, 125: 103646
32. Xia L P, Quan L, Ge L, Hao Y X. Energy efficiency analysis of integrated drive and energy recuperation system for hydraulic excavator boom. Energy Conversion and Management, 2018, 156: 680–687